

Synthesis and characterization of polypyrrole and its application for solar cell

Faisal M. A. Almuntaser¹ · Sutripto Majumder² · Prashant K. Baviskar¹ · Jaydeep V. Sali¹ · B. R. Sankapal²

Received: 6 November 2016 / Accepted: 10 July 2017 / Published online: 29 July 2017
© Springer-Verlag GmbH Germany 2017

Abstract In this report, the fabrication of a solar cell device with the structures FTO/PPy/PTh/ZnO/Al was performed using wet chemical synthesis methods in open environment. The cost-effective methods like CBD, SILAR, and spin coating have been used for the synthesis. The effect of thickness of PPy active layer on the device performance is investigated. Features such as structural, morphological, and chemical bonding of the layers have been investigated using X-ray diffraction, field emission scanning electron microscopy, and Fourier transform infrared spectroscopy and are discussed herein. Effects of PPy thickness on current–voltage characteristics have been studied under dark and illumination at 1 Sun (100 mW/cm², AM 1.5 G) condition to study the solar cell performance.

1 Introduction

Understanding the fact that both depletion and pollution created by the fossil fuel as an energy source, organic solar cells have become the heart of current low-carbon economy which leads us to grow our interest towards the issues related to environmental pollution due to energy crisis [1]. Polymer solar cells have a combination of flexibility and low-cost fabrication, so they are attracting as a possible

application for energy sources. During the last two decades, attempts had been made to fabricate junction devices using conducting polymers as an active material, which replaces the conventional inorganic semiconductors and expensive standard polymers in the fabrication of photo-sensitive junctions in electronic and optical devices, such as solar cells [2].

In this perspective, conducting polymer thin films have received great interest in many application fields because of their mechanical, chemical, and physical properties. It has the characteristics of high sensitivities, short response times, and optimum performance at ambient temperatures. The polythiophene (PTh), polypyrrole (PPy), and polyaniline (PAni), as the conjugate polymers, have attracted more attention for their frequent usage in the energy field as a conducting polymer. Among these, PPy has been known for nearly a century; it is one of the most promising conducting polymer due to its unique properties. Its main advantages are as follows: commercially available, water-soluble, high electrical conductivity, biocompatibility, pH sensitivity, good stability in ambient conditions, and rather easy preparation, where the monomers of pyrrole are easily oxidized [3–6]. The most preferred method of preparation of polymer is either electrochemical or chemical oxidation of monomer in aqueous medium. The synthesis of polymer by either of these methods depends upon the intended application of the polymer. PPy can be easily synthesized either electrochemically or chemically [7, 8]. Nowadays, the preparation of conducting polymer by chemical oxidative polymerization has been developed, since this method is easier and more effective. Chemical synthesis is used for large quantities of material and involves mixing a strong oxidizing agent [9]. In this method, the distribution between polypyrrole and host polymer is good, and thus electrical

✉ B. R. Sankapal
brsankapal@gmail.com; brsankapal@phy.vnit.ac.in

¹ Department of Physics, School of Physical Sciences, North Maharashtra University, Jalgaon, MS 425001, India

² Nano Materials and Device Laboratory, Department of Physics, Visvesvaraya National Institute of Technology, South Ambazari Road, Nagpur, MS 440010, India

conductivity and mechanical properties were increase. The popularity of this method can be attributed to two characteristics namely simplicity and reproducibility.

The basic properties, such as optimal preparative conditions and behavior of PPy during the fabrication, have not been systematically studied [10]. In many reports, it is found that PPy was used as a counter electrode for dye-sensitized solar cells, hole transparent layer in solar cell, photocatalysis, supercapacitors, gas sensor, and fuel cell device applications [11–15].

Therefore, this firms our idea for the construction of nanostructured thin film of PPy for solar cells. Fabrication of any desired nanostructure of polypyrrole (PPy) using hard and soft template methods is still surprisingly challenging for researchers, since for that each fabrication method has its own drawbacks [16]. Hence, low-cost and easy manufacturing methods need to be employed for the fabrication of solar cell device. To the best of our knowledge, there are no other reports about the fabrication of PPy constructed from nanostructured-building blocks using chemical bath deposition. Additionally, this is the first report for the fabrication of a solar cell of FTO/PPy/PTh/ZnO/Al device structure carried out in ambient atmosphere.

2 Experiment part

2.1 Materials

The glass slides coated with fluorine-doped tin oxide (FTO) (thickness 2 mm, sheet resistance $\sim 15 \Omega/\text{cm}^2$) and pyrrole monomer ($\text{C}_4\text{H}_5\text{N}$) were purchased from Sigma Aldrich, zinc acetate ($\text{Zn}(\text{CH}_3\text{COO})_2 \cdot 2\text{H}_2\text{O}$), sulfuric acid (H_2SO_4), and hydrochloric acid (HCl) were purchased from Loba Chemie, whereas ethanol ($\text{C}_2\text{H}_6\text{OH}$) and ammonium peroxydisulfate $[(\text{NH}_4)_2\text{S}_2\text{O}_8]$ from Merck, India. Acetonitrile ($\text{C}_2\text{H}_3\text{N}$) was purchased from Vetec, India, zinc powder and thiophene ($\text{C}_4\text{H}_4\text{S}$) were from Spectro chem., India, and FeCl_3 was from Rankem, India, and all the chemicals were used as received, without any further purification.

2.2 Device fabrication

2.2.1 Preparation of patterned-FTO

Fluorinated tin oxide (FTO) coated glass substrate was etched by spreading zinc powder over the required area of FTO followed by spreading the mix solution of hydrochloric acid and DDW at the ratio of 1:1 over the same. The patterned-FTO was cleaned using the mixture of DDW with 5% nitric acid followed by successive cleaning with liquid soap and acetone, and finally using DDW in an ultrasonic bath for 15 min sonication in each step. The

cleaned substrates were dried in an oven at $150 \text{ }^\circ\text{C}$ for 20 min and then used for synthesis.

2.2.2 Polypyrrole thin film formation

Polymerization was done by purring pyrrole monomer and (ammonium peroxydisulfate) APS solutions simultaneously in a beaker which contained cleaned substrate. PPy polymerization was performed using CBD and the bath contained the mixture of 0.02 M concentration of pyrrole monomer and 1 M concentrated H_2SO_4 prepared in 40 ml of DDW as cationic source. As soon as both of these mix, the polymerization process immediately starts with the appearance of black color which confirms the formation of PPy. Substrate was kept in this bath for 45 min, then removed and rinsed with DDW. This deposition process was repeated for two, three and four cycles on separate substrates. Thick and black films were removed from the bath and rinsed with DDW, and annealed at $120 \text{ }^\circ\text{C}$ for 30 min.

2.2.3 Polythiophene thin film formation

Polymerization of PTh had been done using successive ionic layer adsorption and reaction (SILAR) method which is already reported by Patil et al. through chemical oxidative polymerization of thiophene using FeCl_3 [17]. Briefly, 0.03 M of thiophene was dissolved in acetonitrile with pH ~ 6 and used as cationic solution, whereas 0.06 M of anhydrous ferric chloride FeCl_3 was used as anionic solution. Thin film deposition of PTh was taken place by immersing FTO-coated PPy film for 15 s in thiophene and ferric chloride solution, alternatively. This process was repeated for 20 cycles. To get good crystallinity, the films were annealed at $150 \text{ }^\circ\text{C}$ for 30 min.

2.2.4 Deposition of zinc oxide layer and aluminum back contact

Thin film of zinc oxide (ZnO) was deposited using spin coating method by following the recipe described by Li et al. [18]. In short, zinc acetate with 0.015 M was made in the ethanol and stirred for 1 h at room temperature ($27 \text{ }^\circ\text{C}$). Finally, the mixture was dropped over the PPy/PTh grown films, and spin-coated at 3000 rpm for 30 s. Ohmic contacts of aluminum (Al) with the thickness of 100 nm was deposited over PPy/PTh/ZnO thin films using thermal evaporation method, which was operated under vacuum of 5×10^{-4} Torr.

Figure 1 shows the schematic diagram of the device with FTO/PPy/PTh/ZnO/Al structure. The thickness of PTh over PPy film was found to be 130 nm, whereas about 45 nm of ZnO was deposited on the top of the PTh layer.

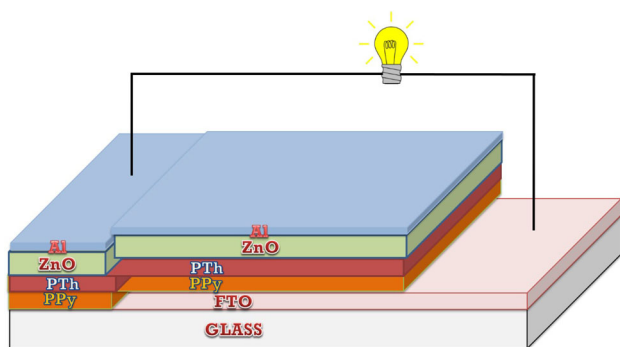


Fig. 1 Schematic diagram of fabricated solar cell device

Finally, for back contact, 100 nm of aluminum was deposited using thermal evaporation method.

3 Characterizations

The surface morphology of the samples was studied using field emission scanning electron microscope (HITACHI S-4800) operated at 15 kV coupled with an energy dispersive X-ray spectroscopy (EDX) unit. The structural analysis of the prepared samples was performed using XRD; Bruker (Model: D8 advance) with CuK_α radiations ($\lambda = 1.54 \text{ \AA}$). The UV–Vis spectrophotometer (UV1600, Shimadzu) was used to record the absorbance spectra for optical studies of resulting films. Dektak-150 surface profiler was used for measuring the thickness. The photovoltaic performances of the devices were recorded using current–voltage source/sink measurement unit (Keithley-2611A) with exposed area of 0.1 cm^2 regulated by mask under dark and illumination conditions of AM 1.5 G at 100 mW/cm^2 . Fourier transform infra-red (FTIR) spectra were recorded using a Perkin Elmer FTIR to analyze the formation of different chemical bonding in the deposited films.

4 Results and discussion

4.1 Surface morphology and elemental analysis

Figure 2a shows the image of PPy nanostructured thin film covered over the FTO substrate at higher magnification, whereas Fig. 2b shows the image at lower magnification for three CBD cycles. From Fig. 2b, it is quite evident that PPy particles combine to form a uniform globular-like structure of PPy coated over FTO. Along with this, there were no cracks or pin holes found to appear in the morphology of the obtained film. The advantage of the porous substrate is to improve electrocatalytic activity of the film.

Apart from this, it is also found that this globular type of structure conglomerated, which makes them interconnected to each other [19]. Similar type of structure is also reported by Bulakhe et al. [20]. Figure 2c, d shows the morphology of PPy film was completely covered with the other two layers of PTh and ZnO, respectively. Figure 2e, f describes the purity and composition of the prepared samples using elemental analysis by EDX spectra. The existence of elements Zn (from ZnO), O (from both ZnO and pyrrole), and Fe (from PTh) was observed in the result. Also, the EDX spectrum of the composite material film shows a signal of carbon (C) at 0.25 keV and oxygen (O) at 0.52 keV, which represents the existence of the PPy polymer. The presence of lone pair-free electrons of Fe is attributed to the reaction of the FeCl_3 on the weak bonds of thiophene monomer. Hence, the polymerization process of polythiophene becomes rapid and the formation of chain of polythiophene takes place very fast with agglomeration of polythiophene polymer to form globular grains [21].

4.2 Structural studies

The presence of PPy microcrystalline structures in the prepared PPy film, and film composite of PPy, PTh, and ZnO fabricated for device are confirmed from XRD studies shown in Fig. 3. The broad peak observed at 24.5° is a characteristic peak of amorphous PPy [pattern (a)] which is found to be similar to that observed by Partch et al. [22]. The crystallite size (D) of PPy nanoparticles was calculated from the major diffraction peak of the corresponding PPy using the Debye–Scherer formula from the relationship:

$$D = \frac{k\lambda}{\beta \cos\theta} \quad (1)$$

The interplanar spacing between PPy planes was calculated using the following formula:

$$2d \sin\theta = n\lambda, \quad (2)$$

where k is a constant, often taken as 0.9, λ is the wavelength of X-ray, i.e. 1.54 \AA value for the $5.9 \text{ keV CuK}_\alpha$ X-ray radiation source, θ is the diffraction angle of incident light, and β is the full width at half maximum (FWHM) of the prominent peak. The crystallite size was found to be 1.748 nm , whereas interplanar spacing ‘ d ’ between PPy planes is 7.27 nm .

Song et al. referred that the high intense peak appeared at 26° which shows the doping level and the type of dopant. Along with this, the short-range ordering of PPy influences the intensity of peaks at high angle, which becomes more distinct with shorter chain length of dopants. Therefore, the higher conductivity resulted from the ordering of PPy chains for shorter dopant systems [8].

Fig. 2 FE-SEM image of PPy for **a** and **b** three CBD cycles, **c** and **d** FE-SEM image of the top surface of ZnO over PPy/PTh, **e** EDX spectrum of three CBD cycles of PPy thin film and **f** ZnO thin film infiltrated with the active layer (PPy/PTh)

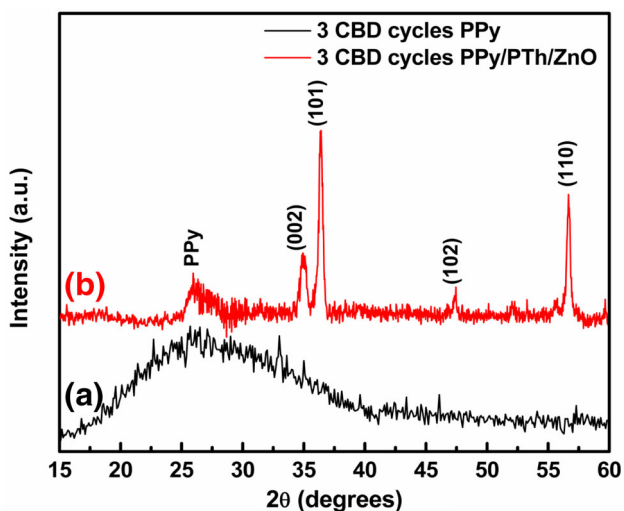
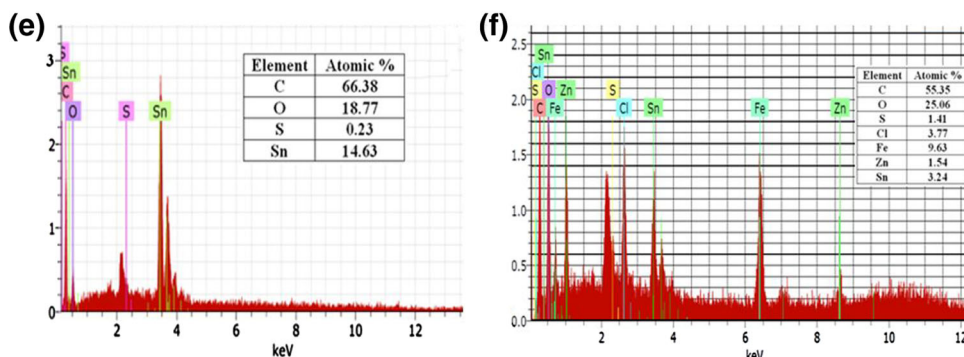
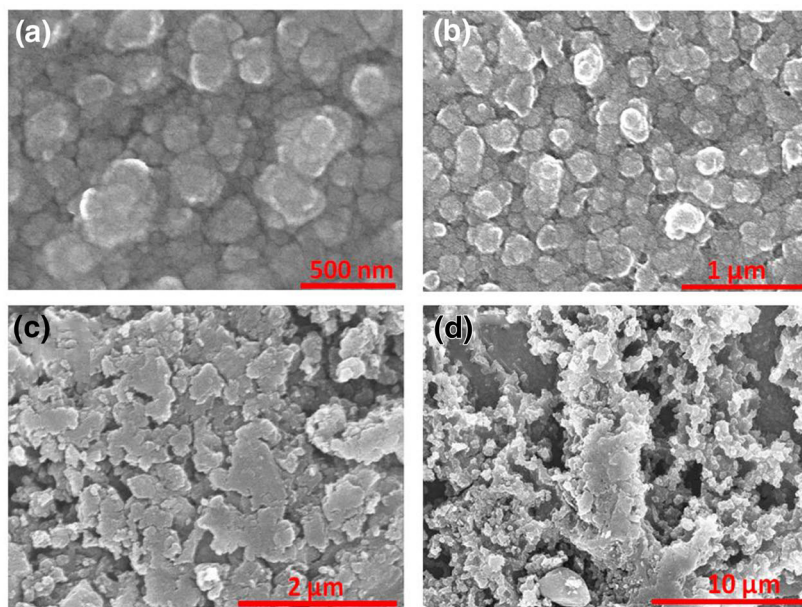


Fig. 3 **a** X-ray diffraction pattern of pure PPy, which has a broad peak at about $2\theta = 24.5^\circ$ and **b** the XRD of the fabricated device

Again from Fig. 3 pattern (b) for 3 CBD cycles, PPy/PTh/ZnO shows a broad characteristic peak at $2\theta = 25^\circ$ which implies the presence of PPy and exhibits an

amorphous structure [23]. Ashokan et al. revealed that the broad diffraction peak observed at $2\theta = 20^\circ$ to the crystalline nature of doped-PPy [24].

The emergence of amorphous nature of X-ray diffraction (XRD) pattern for PTh indicates the intermolecular stacking structure as well as amorphous packing of the relatively smooth grains which were distributed randomly [17]. The examined crystal structure of the ZnO was verified by the diffraction peaks of ZnO nanoparticles which were indexed as 34.88° (002), 47.45° (102), and 56.67° (110), this indicates that the as-grown ZnO nanoparticles are almost grown in a direction perpendicular to the substrate surface along the *c*-axis. All diffraction peaks of sample correspond to the characteristic hexagonal wurtzite structure of ZnO nanoparticles [25].

4.3 Optical studies

The UV-Vis absorption spectrum of the PPy films and devices was recorded, as shown in Fig. 4. From Fig. 4a, PPy-doped sulfuric acid of two CBD cycles shows three

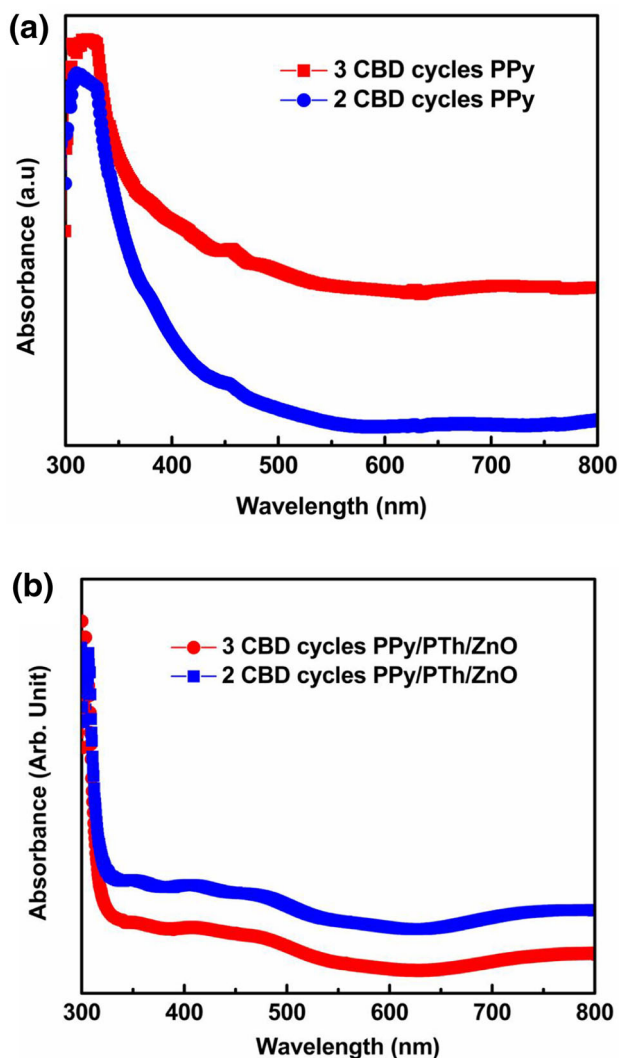


Fig. 4 UV-Vis of **a** pure PPy film and **b** the fabricated devices with three CBD cycles PPy

characteristic peaks of absorption in wavelength at 317.5 and in the range 452.5–453.5 and 661–684 nm, respectively. The peak at wavelength of 317.5 nm is due to the π - π^* electron orbital transition of benzenoid ring along the backbone of the PPy chains [26]. The peak in wavelength range of 661–684 nm is attributed to the π -polaron transition. The peak of wavelength band 452.5–453.5 nm is due to the polaron- π^* transition, where at this wavelength range, the emergence of n - π^* transitions also exists owing to electrons in nonbonding orbitals of the amino nitrogen which is formed by the quinoid rings [27, 28]. The prominent direct band gaps are around 1.85 eV for middle of wave length absorption 684–661 nm and 2.74 eV for middle of 452.5–453.5 nm (first- and second-order transitions) of PPy of two cycles CBD.

Similarly, for three cycles of CBD-PPy-doped sulfuric acid, it shows three characteristic peaks of absorption in

wavelength bands 321.5, 454–456, and 700–721 nm, respectively. The reason for the formation of these three peaks has been described earlier in this section. But noticeably, it can be seen that all the peaks are found to be red shifted in their wavelength ranges. This clarifies that the more growth of the PPy layer is due to increase in one more round of CBD method for PPy deposition. As a result of which, increase in the grain size takes place. The band gap is around 2.73 eV for middle of 454–456 nm (first- and second-order transitions) of three cycle PPy, as shown in Fig. 4a. The prominent direct band gaps are around 1.75 eV for middle of wave length absorption 700–721 nm and this matches well with reported result [7].

PPy is bipolaron formation polymer due to its highly disordered structure (one defect in every three rings). Bipolaron formation takes place when two polarons are formed on the same chain; the polarons are independent and not bound to each other [29]. Now from Fig. 4b, it can be found that the variation of optical absorbance of polythiophene thin film on PPy with incident photon wavelength showed the same result as previously reported [17], with π - π^* electron orbital transition of benzenoid ring at 306 nm [28], whereas the peak at 375 nm shows the band gap of ZnO corresponding to 3.3 eV at room temperature. In case of PPy-PTh-ZnO thin films, the broad peak around 400–520 nm is ascribed to the selective interaction between ZnO and quinoid ring of PPy with increased intensity of the peak compared to pure PPy. Also, the peaks of PPy-ZnO, observed in UV-Vis spectra, may be attributed to the interactions between PPy chains and ZnO nanoparticles which cause easy charge transfer from PPy to ZnO via hydrogen bonding [30].

4.4 Fourier transform infra red (FTIR) spectroscopy

The FTIR spectra of three CBD cycle PPy film and the device deposited over the same, PPy/PTh/ZnO are recorded as a function of wave number in the range 4000–500 cm^{-1} and illustrated in Fig. 5a and b, respectively. Band present at the peak 581 cm^{-1} is due to C-S stretching vibration, and the broad peak at 1338 cm^{-1} confirms C-C and C-N vibration modes [31]. The absorption band peaks present at 986 cm^{-1} and 1091 cm^{-1} correspond to C-C out-of-plane ring deformation vibration and in-plane deformation vibration of N-H, respectively [32]. Band appeared at 1637 cm^{-1} is attributed to the bending mode of H-O-H [33]. The band present at 1554 cm^{-1} corresponds to the pyrrole ring vibrations [34]. The IR peak observed at 888 cm^{-1} may be assigned to the =C-H out-of-plane vibration indicating polymerization of pyrrole and 1338 cm^{-1} may correspond to =C-H band in-plane vibration [35]. The decrease in long absorption from

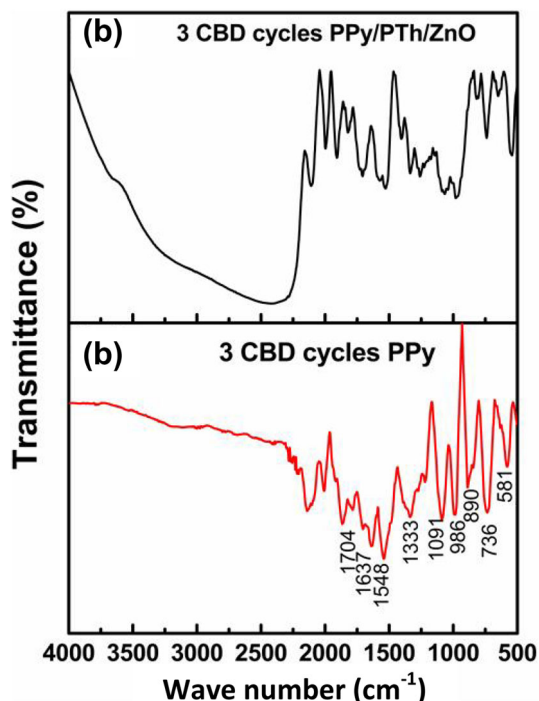


Fig. 5 FTIR of **a** pure PPy and **b** the device of three CBD cycles PPy

4000 to about 1700 cm^{-1} has been assigned to the tail of an absorption peak located in the region near, for oxidized PPy [36].

From Fig. 5b it can be found that the bands at 582 cm^{-1} are characteristics of C–H out-of-plane bending vibrations of benzene nuclei of PPy [37]. The broad peak band between 350 and 600 cm^{-1} is assigned to Zn–O stretching, and stretching vibrations at 1528 cm^{-1} are assigned to C=C of PPy [24]. Band of peak at 1405.95 cm^{-1} belongs to C–C symmetric stretching vibration modes of thiophene ring and 1066 cm^{-1} is assigned to C–H in-plane deformation for PTh [17]. PPy–PTh–ZnO nanocomposite illustrated that PPy had successfully incorporated with addition of PTh/ZnO and over the PPy rings the localization of strong electrons gets highly reduced from oxidized form [30]. Thus, the FTIR spectra confirm the formation of polypyrrole deposited using chemical bath deposition. This also confirms the existence of all deposited materials in between the conducting electrodes of fabricated three cycle PPy device.

4.5 Current density–voltage (J – V) characterization

The J – V characteristics of the thin film solar cell (Fig. 6) exhibit considerable photovoltaic performance for three cycle PPy device under illumination AM 1.5 G ($\sim 100\text{ mW/cm}^2$, 1 sun). Using the photovoltaic curves under illumination, the output parameters were calculated using the following relations [38]:

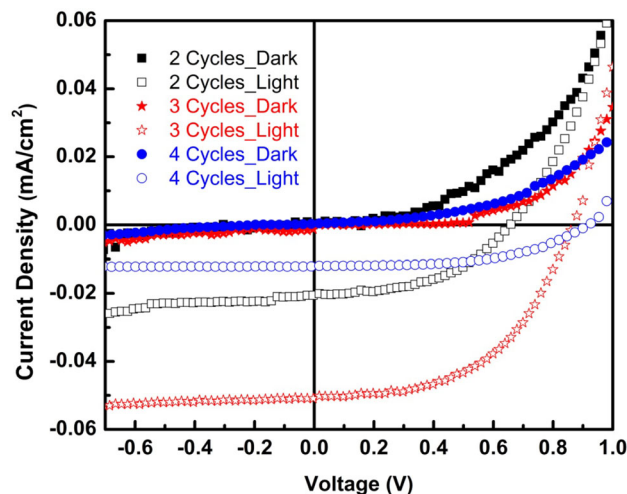


Fig. 6 J – V characteristics under dark and illumination of device PPy/PTh/ZnO/Al with two, three, and four CBD cycles of PPy

$$\eta = \frac{V_{OC} \times J_{SC} \times FF}{P_{in}} \times 100\% \quad (3)$$

$$FF = \frac{I_M \times V_M}{I_{SC} \times V_{OC}} \quad (4)$$

where P_{in} stands for input power of light energy and I_M and V_M are values of maximum current and voltage at the maximum power point, respectively. The series and shunt resistance were calculated from the slope of the output power characteristics using the relations:

$$\left[\frac{dI}{dV} \right]_{I=0} = \frac{1}{R_S} \quad (5)$$

$$\left[\frac{dI}{dV} \right]_{V=0} = \frac{1}{R_{Sh}} \quad (6)$$

It is observed that with increase in CBD cycles of PPy from two to three there is an enhancement in the performance of device. From table, it is observed that with increase in number of CBD cycles for PPy the values for J_{sc} and the efficiency of device increase up to three cycles. The low values of J_{sc} for device with two cycles might be due to the non-uniform coverage of PPy results in the improper junction formation which is responsible for low performance of device. On the other hand, for four cycles the PPy layer gets peeled off, this results in lowering the performance of device. Power conversion efficiency (PCE) of the device for three cycle PPy is 0.0227%, which shows a maximum overall performance compared to the device with two and four PPy cycles. This may attribute to better charge collection efficiency and enhance the conductivity mechanism through the increasing formation of bipolarons and polarons. This increases with increasing number of hole transport to aluminum electrode with thickness increasing of polypyrrole up to three cycles. The

Table 1 Photovoltaic output parameters derived from the J - V characterization of the fabricated devices

Label	J_{sc} (mA/cm ²)	V_{oc} (V)	J_{max} (mA/cm ²)	V_{max} (V)	R_s (k Ω)	R_{sh} (k Ω)	FF (%)	PCE (%)
Two CBD cycle PPy device	0.020	0.655	0.015	0.425	4.174	44.518	48	0.006
Three CBD cycle PPy device	0.050	0.862	0.039	0.572	3.774	67.006	51	0.022
Four CBD cycle PPy device	0.012	0.919	0.009	0.622	5.268	51.109	53	0.005

photovoltaic parameters, such as short circuit current density (J_{sc}), open circuit voltage (V_{oc}), maximum current density (J_{max}), maximum voltage (V_{max}), series resistance (R_s), shunt resistance (R_{sh}) fill factor (FF), and power conversion efficiencies (PCE) were calculated and tabulated as in Table 1.

The amorphous thin film structures were deposited at room temperature in an ambient condition. As the film thickness increases due to increase in CBD cycles from two to three of PPy, the grain size becomes bigger and it can be concluded that the concentration of electrical carrier increases, and thus the electrical resistivity decreases with an increase in the film thickness [5]. It was also observed that the conductivity of the device increases due to the presence of ZnO with PPy [24]. Somani et al. shows that the reduction in the band gap energy of polymer can be achieved due to the doping effect. This is found quite resembling to our case, where the growth of ZnO over PPy/PTh tunes the band alignment, and hence creates the bipolaronic conduction band through lowering the energy level of the conduction band [39]. The low value of overall conversion efficiency of fabricated devices may attribute due to poor carrier mobility in the layer-by-layer films which contain many ionic units that act as the trap states for the charges, and this combined with the relatively low optical cross section of the materials in the visible region [40].

5 Conclusion

Complete solid-state devices of ZnO-conducting polymers [polypyrrole (PPy) and polythiophene (PTh)] were fabricated. The devices designed with conventional structures of FTO/PPy/PTh/ZnO/Al were fabricated using simple and low-cost chemical routes, namely, chemical bath deposition method (CBD), successive ionic layer adsorption and reaction (SILAR), and spin coating. It has been found that on increasing the number of CBD cycles of PPy can actively harvest the visible light matching the semiconductor energy levels. Except this, the highest open-circuit voltage achieved was 0.919 V with four CBD cycle PPy solar cell. These results may attribute to the thickness of the PPy during

fabrication process. The low value of conversion efficiency of fabricated devices may attribute to relatively low optical absorbance of the conducting polymers in the visible region and this combined with presence of the ionic units in the layer-by-layer films that trap charges and reduce the number of charges. The photovoltaic performance and the rectification behavior of the devices presented above suggest a successful formation of a heterojunction of fabricated device layers.

Acknowledgements We thank NMU Jalgaon and VNIT Nagpur for all help and support, also FMAA thanks Aden University Yemen for the financial support.

References

1. J. Wu, Y. Li, Q. Tang, G. Yue, J. Lin, M. Huang, L. Meng, *Sci. Rep.* **4**, 4028 (2014)
2. Y. Hao, M. Yang, W. Li, X. Qiao, L. Zhang, S. Cai, *Sol. Energ. Mat. Sol. Cells* **60**, 349 (2000)
3. F.G. İnce, S. Şen, Z. Özbek, H. Göktaş, M.E. Öze, R. Çapan, *J. Optoelectron. Adv. Mater.* **11**, 1182 (2009)
4. S.H. Hosseini, A. Asadnia, *J. Nanomater.* **2012**, 198973 (2012)
5. A.R.N. Laily, M.I.N. Isa, H. Salleh, S. Hasiyah, *ECS J. Solid State Sci. Technol.* **19**, 107 (2011)
6. P. Galář, B. Dzurňák, P. Malý, J. Čermák, A. Kromka, M. Omastová, B. Rezek, *Int. J. Electrochem. Sci.* **8**, 57 (2013)
7. J.V. Thombare, S.K. Shinde, G.M. Lohar, U.M. Chougale, S.S. Dhasade, H.D. Dhaygude, B.P. Relekar, V.J. Fulari, *J. Semicond.* **35**, 063001 (2014)
8. M.K. Song, Y.T. Kim, B.S. Kim, J. Kim, K. Char, H.W. Rhee, *Synth. Met.* **141**, 315 (2004)
9. D.D. Ateh, H.A. Navsaria, P. Vadgama, *J.R. Soc. Interface* **3**, 741 (2006)
10. E.L. Kupila, J. Kankare, *Synth. Met.* **74**, 241 (1995)
11. X. Ma, G. Yue, J. Wu, Z. Lan, *Nanoscale Res. Lett.* **10**, 327 (2015)
12. Z. Zhang, W. Wang, E. Gao, *J. Mater. Sci.* **49**, 7325 (2014)
13. P.M. Kharade, S.M. Mane, S.B. Kulkarni, P.B. Joshi, D.J. Salunkhe, *J. Mater. Sci.: Mater. Electron.* **27**, 3499 (2016)
14. P. Patil, G. Gaikwad, D.R. Patil, J. Naik, *Bull. Mater. Sci.* **39**, 655 (2016)
15. M.H. Seo, E.J. Lim, S.M. Choi, H.J. Kim, W.B. Kim, *Top. Catal.* **53**, 678 (2010)
16. D.P. Dubal, Z. Caban-Huertas, R. Holze, P. Gomez-Romero, *Electrochim. Acta* **191**, 346 (2016)
17. B.H. Patil, A.D. Jagadale, C.D. Lokhande, *Synth. Met.* **162**, 1400 (2012)
18. Y. Li, J. Gong, M. McCune, G. He, Y. Deng, *Synth. Met.* **160**, 499 (2010)

19. J. Wu, Q. Li, L. Fan, Z. Lan, P. Li, J. Lin, S. Hao, J. Power Sourc. **181**, 172 (2008)
20. R.N. Bulakhe, S.V. Patil, P.R. Deshmukh, N.M. Shinde, C.D. Lokhande, Sens. Actuator B Chem. **181**, 417 (2013)
21. S.V. Kamat, V. Puri, R.K. Puri, Mater. Chem. Phys. **132**, 228 (2012)
22. R.E. Partch, S.G. Gangoli, E. Matijevic, W. Cai, S. Araj, J. Colloid Interface Sci. **144**, 27 (1991)
23. N. Su, H.B. Li, S.J. Yuan, S.P. Yi, E.Q. Yin, Express Poly. Lett. **6**, 697 (2012)
24. S. Ashokan, V. Ponnuswamy, P. Jayamurgan, Int. J. Pharm. Biol. Sci. **1**(5), 261 (2012)
25. H. Kumar, R. Rani, Int. Lett. Chem. Phys. Astron. **14**, 26 (2013)
26. S. Sakthivel, A. Boopathi, J. Chem. Chem. Sci. **4**(3), 144 (2014)
27. P.P. Zamora, M.B. Camarada, I.A. Jessop, F.R. Díaz, M.A. del Valle, L. Cattin, G. Louarn, J.C. Bernede, Int. J. Electrochem. Sci. **7**, 8276 (2012)
28. H.S. Abdulla, A.I. Abbo, Int. J. Electrochem. Sci. **7**, 10666 (2012)
29. O. Ala, Q. Fan, Research Journal of Textile and Apparel **3**, 51 (2009)
30. M.A. Chougule, D.S. Dalavi, S. Mali, P.S. Patil, A.V. Moholkar, G.L. Agawane, J.H. Kim, S. Sen, V.B. Patil, Measurement **45**(8), 1989 (2012)
31. P. Jayamurgan, V. Ponnuswamy, S. Ashokan, T. Mahalingam, Int. J. Thin Film Sci. Tec. **2**, 261 (2013)
32. J.V. Thombare, M.C. Rath, S.H. Han, V.J. Fulari, Materials Physics and Mechanics **16**, 118 (2013)
33. X. Li, J. Sun, G. He, G. Jiang, Y. Tan, B. Xue, J. Colloid Interface Sci. **411**, 34 (2013)
34. D.P. Dubal, S.V. Patil, A.D. Jagadale, C.D. Lokhande, J. Alloy. Comp. **509**, 8183 (2011)
35. T.K. Vishnuvardhan, V.R. Kulkarni, C. Basavaraja, S.C. Raghavendra, Bull. Mater. Sci. **29**, 77 (2006)
36. E.T. Kang, T.C. Tan, K.G. Neoh, Y.K. Ong, Polymer **27**, 1958 (1986)
37. M. Sangareswari, M.M. Sundaram, J. Nanosci. Nanotechnol. **1**(1), 9 (2015)
38. S. Majumder, P.K. Baviskar, B.R. Sankapal, Ceram. Int. **42**, 6682 (2016)
39. P.R. Somani, S. Radhakrishnan, Chem. Phys. Lett. **379**, 401 (2003)
40. T.A. Skotheim, J.R. Reynolds, *Handbook of conducting polymers, Vol 2, Ch 14*, 3rd edn. (Taylor and Francis, New York, 2007), p. 24